

# **Dynamic Interactions between the Ground Heat Exchanger and Environments in Earth-Air Tunnel Ventilation of Buildings**

Guohui Gan

Department of Architecture and Built Environment, University of Nottingham, University Park, Nottingham NG7 2RD, UK

Tel: +44 (0)115 9514876

guohui.gan@nottingham.ac.uk

## **ABSTRACT**

Earth-air tunnel ventilation is an energy efficient method of preheating or cooling of supply air to a building. The purposes of this study are to investigate the performance of earth-air heat exchangers under varying soil and atmosphere conditions and the interactions between the heat exchanger and environments. A computer program has been developed for simulation of the thermal performance of an earth-air heat exchanger for preheating and cooling of supply air, taking account of dynamic variations of climatic, load and soil conditions. The program solves equations for coupled heat and moisture transfer in soil with boundary conditions for convection, radiation and evaporation/condensation that vary with the climate both at the soil top surface and inside the heat exchanger. The importance of dynamic interactions between the heat exchanger, soil and atmosphere is illustrated from the comparison of the heat transfer rates through the heat exchanger. The predicted heat transfer rate varies with operating time and decreases along the passage of air in the heat exchanger. Neglecting the interactions would significantly over-predict the heat transfer rate and the amount of over-prediction increases with operating time.

**KEYWORDS:** Ground heat exchanger, earth-air tunnel ventilation, energy efficient heating, heat transfer, moisture transfer, soil texture, thermal property.

## **1 INTRODUCTION**

Earth-air tunnel ventilation is considered to be an energy efficient means of preheating and cooling of supply air to a building. A key component of a tunnel ventilation system is a ground or earth-air heat exchanger (EAHX) composed of a series of pipe or duct buried below ground for transferring heat between the supply air in the pipe and the surrounding soil with a relatively stable temperature. The heat exchanger can be made of concrete, metal or plastic and the most commonly used material is plastic such as high density polyethylene for small pipes and concrete for large pipes.

The concept of using the stable soil temperature for preheating or cooling of air for building ventilation has been tested since the ancient Greek and Persian times. One of the first modern applications of EAHX was for agricultural buildings such as greenhouses [1-4]. In recent years, the EAHX system has been applied to different types of building in different climates. Breesch et al. [5] used an EAHX for winter preheating and summer precooling of an office building in Belgium. Al-Ajmi et al. [6] showed that an EAHX could potentially reduce cooling energy demand by 30% over the peak summer season for a typical house in a hot and arid climate in Kuwait. The thermal behavior of EAHXs has also been studied for a unique building called 'Casa Ventura' in Brazil [7] and for buildings under three different climatic conditions in Mexico [8]. Because EAHX systems alone are often insufficient to meet the thermal comfort requirements in summer conditions, Misra et al. [9] used a hybrid EAHX to enhance the efficiency of an air conditioner in India whereas Bansal et al. [10] integrated an evaporative cooler with an EAHX to minimise the use of an air conditioner.

The performance of earth-air heat exchangers has been investigated by many researchers using analytical or numerical techniques validated with experimental measurements. Bisioniya et al. [11] have recently provided a review on experimental and analytical studies of EAHX systems. The simplest analytical model is based on the thermo-hydraulic analysis of the EAHX for given soil and air properties [12]. To take account of the daily and seasonal variations of soil and air temperatures, a set of analytical equations representing the effects of climate and soil properties can be incorporated into this type of model [13]. Analytical models are generally based on the simplified solution of one dimensional (axi-symmetrical) heat transfer in a circular pipe or the surrounding soil of homogeneous properties. Different forms of analytical models have been developed to predict the heat transfer through the ground heat exchanger systems [14-16]. However, heat and moisture transfer in shallow soil surrounding a heat exchanger is neither axi-symmetric normal to the pipe nor varying uniformly along the pipe for long term operation due to the influence of daily and seasonal climatic variations and interactions between soil and the heat exchanger. For more realistic simulation, therefore, numerical solution of a three-dimensional model is required and this type of numerical heat transfer model has been developed or applied by a number of researchers [17-21] to predict the performance of EAHXs. Both analytical and numerical models allow parametric analysis to be performed such as air and soil properties and pipe size but the numerical model would also enable additional parameters such as non-uniform soil properties and pipe configurations to be analysed. Tzaferis et al. [22] compared eight different heat transfer models for evaluating the performance of EAHXs and found that most of them gave rise to similar results and that all of them were able to predict the general trend of the performance in terms of the outlet air temperature but none of them was accurate for predicting the patterns of daily variation.

In an earth-air tunnel ventilation system, simultaneous heat and moisture transfer could occur in soil and in the pipe. Hollmuller and Lachal [23] developed a numerical model for the sensible and latent heat transfer inside the ground pipe and examined the potential of the ground pipe systems for winter preheating and summer cooling. Gauthier et al. [24] not only developed a three-dimensional model for heat transfer in soil but also accounted for the sensible and latent heat transfer in the heat exchanger. Based on the work of Puri [25], Santamouris et al [2] and Mihalakakou et al [26] developed an axi-symmetric model of heat and mass transfer for the calculation of temperature and moisture in the pipe and soil and this was used for the prediction of the thermal performance of EAHXs. Darkwa et al. [27] also presented equations for axi-symmetric heat and moisture transfer in soil but did not provide the solution. Instead, the soil temperature was obtained from the analytical model developed by Lee and Strand [13] for evaluating the performance of an earth-air ventilation system.

This study aims to develop a numerical model for the simulation of transient heat and moisture transfer in soil with a horizontally coupled EAHX for preheating and cooling of buildings. The model takes account of interactions of heat and moisture transfer in soil and between the soil, heat exchanger, supply air (air passing through the heat exchanger) and ambient conditions.

## **2 THEORY**

Simulation of simultaneous heat and moisture transfer in a system of earth, air and heat exchanger is carried out through numerical solution of energy and mass conservation equations for soil together with the heat and mass balance as the boundary conditions at the interfaces between earth and atmosphere and between the heat exchanger and supply air.

## 2.1 Model Equations

The transient heat and moisture transfer in soil with phase change is represented by the following coupled energy and mass conservation equations:

$$\frac{\partial(\rho CT)}{\partial t} = \nabla \left( (k + L\rho_l D_{T,v}) \nabla T \right) + \nabla (L\rho_l D_{\Theta,v} \nabla \Theta) + q_v \quad (1)$$

$$\frac{\partial \Theta}{\partial t} = \nabla \left( (D_{T,l} + D_{T,v}) \nabla T \right) + \nabla \left( (D_{\Theta,l} + D_{\Theta,v}) \nabla \Theta \right) + \frac{\partial K}{\partial z} + \Theta_v \quad (2)$$

where  $\rho$ ,  $C$  and  $k$  are the density ( $\text{kg/m}^3$ ), specific heat ( $\text{J/kgK}$ ) and thermal conductivity ( $\text{W/mK}$ ) of soil, respectively;  $T$  is the temperature of soil ( $\text{K}$ );  $t$  is the time ( $\text{s}$ );  $L$  is the latent heat of vaporisation (for evaporation/condensation) or fusion of water (for freezing/thawing) ( $\text{J/kg}$ );  $\rho_l$  is the density of liquid (ie water) ( $\text{kg/m}^3$ );  $\Theta$  is the volumetric moisture content ( $\text{m}^3/\text{m}^3$ );  $q_v$  is the volumetric heat production/dissipation rate ( $\text{W/m}^3$ );  $D_{T,l}$  and  $D_{T,v}$  are the thermal liquid and vapour moisture diffusivities, respectively, ( $\text{m}^2/\text{sK}$ );  $D_{\Theta,l}$  and  $D_{\Theta,v}$  are the isothermal liquid and vapour moisture diffusivities, respectively, ( $\text{m}^2/\text{s}$ );  $K$  is the hydraulic conductivity of soil ( $\text{m/s}$ );  $z$  is the vertical coordinate ( $\text{m}$ );  $\Theta_v$  is the source/sink of moisture ( $\text{m}^3/\text{m}^3\text{s}$ ).

The moisture diffusivities are defined as follows:

$$D_{T,l} = K \frac{\partial \Psi}{\partial T} \quad (3)$$

$$D_{T,v} = D_v \alpha f(\Theta) \frac{1}{\rho_l} \frac{\partial \rho_v}{\partial T} \quad (4)$$

$$D_{\Theta,l} = K \frac{\partial \Psi}{\partial \Theta} \quad (5)$$

$$D_{\Theta,v} = D_v \alpha f(\Theta) \frac{1}{\rho_l} \frac{\partial \rho_v}{\partial \Theta} \quad (6)$$

The matric potential  $\Psi$  (in m) and hydraulic conductivity of soil  $K$  are given by the following pedo-transfer functions of moisture content [28 and 29]

$$\Psi = \Psi_s \left( \frac{\Theta}{\Theta_s} \right)^b \quad (7)$$

$$K = K_s \left( \frac{\Theta}{\Theta_s} \right)^{2b+3} \quad (8)$$

In Equations (3) to (8),  $b$  is constant dependent on the type of soil,  $D_v$  is the diffusion coefficient of water vapour in air ( $\text{m}^2/\text{s}$ ),  $f(\Theta)$  is the fractional volume of gas-filled pores ( $f(\Theta) = \Theta_s - \Theta$ ),  $K_s$  is the saturated hydraulic conductivity ( $\text{m/s}$ ),  $\alpha$  is the tortuosity factor for diffusion of gases in soil,  $\Psi_s$  is the saturated matric potential or capillary pressure ( $\text{m}$ ),  $\Theta_s$  is the saturated volumetric moisture content ( $\text{m}^3/\text{m}^3$ ) and  $\rho_v$  is the density of water vapour ( $\text{kg/m}^3$ ).

The thermal and physical properties of a soil mixture can vary with temperature, location and time as well as its constituents such as the moisture content. The density, specific heat and thermal conductivity of a soil mixture are represented by the following functions of the volumetric composition of dry solid matter and three phases of moisture – liquid water, water vapour and solid ice:

$$\rho = \rho_d \theta_d + \rho_l \theta_l + \rho_i \theta_i + \rho_p \theta_p \quad (9)$$

$$\rho C = \rho_d C_d \theta_d + \rho_l C_l \theta_l + \rho_i C_i \theta_i + \rho_p C_p \theta_p \quad (10)$$

$$k = \frac{k_l \theta_l + f_i k_i \theta_i + f_p k_p \theta_p + \sum_{m=1}^n f_m k_m \theta_m}{\theta_l + f_i \theta_i + k_p \theta_p + \sum_{m=1}^n f_m \theta_m} \quad (11)$$

where  $\theta$  is the volumetric fraction of a constituent; subscripts d, l, i and p represent dry soil, liquid moisture, ice and gas-filled pores, respectively, and m is the m<sup>th</sup> component of dry soil.  $f_i$ ,  $f_p$  and  $f_m$  are the ratios of the average temperature gradient of the constituent (ice, pores and the m<sup>th</sup> component of n types of dry soil grains) to that of water and are given by the following equation [30]:

$$f_x = \frac{1}{3} \sum_{j=a}^c \left[ 1 + \left( \frac{k_x}{k_l} - 1 \right) g_j \right]^{-1} \quad (12)$$

where subscript x is i, p or m;  $g_a$ ,  $g_b$  and  $g_c$  depend on the ratios of the axes of the grains and the sum of them equals to unity.

The thermal conductivity of pores is influenced by dry air ( $k_a$ ) and the phase change of moisture:

$$k_p = k_a + LD_v \phi \frac{p_{atm}}{p_{atm} - p_v} \frac{d\rho_{vs}}{dT_v} \quad (13)$$

where  $\phi$  is the relative humidity of soil air,  $p_{atm}$  is the atmospheric pressure (Pa),  $p_v$  is the partial pressure of water vapour (Pa),  $\rho_{vs}$  is the density of saturated water vapour ( $\text{kg/m}^3$ ) and  $T_v$  is the temperature of water vapour (K).

The thermal conductivity of soil could also be estimated using empirical relationships with soil moisture content such as the following expression developed by Lu et al [31]:

$$k = (k_{sat} - k_d) \exp \left( a \left( 1 - \left( \frac{\Theta}{\Theta_s} \right)^{a-1.37} \right) \right) + k_d \quad (14)$$

where  $k_{sat} = \left( k_{qz}^{qc} k_o^{1-qc} \right)^{1-\Theta_s} k_l^{\Theta_s}$ ;  $k_d = 0.51 - 0.56\Theta_s$ ;  $k_l$ ,  $k_{qz}$  and  $k_o$  are the thermal conductivities of water, quartz and minerals other than quartz, respectively, (W/mK); and superscript qc represents the quartz content in soil.

The calculated thermal conductivities using the two methods for a range of moisture contents of soil with loam texture (its details given later) are shown in Fig. 1 where  $k_{dV}$  and  $k_{Lu}$  are the conductivities from Equations 11 and 14, respectively. It is seen that the two methods would give rise to similar values at moderate to high moisture contents. The thermal conductivity calculated using the de Vries' method is slightly higher but the difference is less than 1% near the middle of the range. The expression by Lu et al is simpler but it could not account for the influence of the phase change of moisture (vapour distillation or liquid freezing) on the thermal conductivity.

The partial differential equations (1) and (2) are solved for a three-dimensional model using the control volume method with the initial and boundary conditions described below. The computational domain is rectangular and a heat exchanger is represented by a series of parallel

pipes inside the domain. Fig. 2 shows a vertical section normal to one pipe of the heat exchanger.

## 2.2 Initial Conditions

The initial soil temperature at time  $t = t_0$  and the far-field temperature at any time  $t$  (day) and depth  $Z$  (m) are given by,

$$T = T_m - T_{amp} e^{-Z/D} \sin\left((t - t_0) \frac{2\pi}{365} - \frac{Z}{D} - \frac{\pi}{2}\right) \quad (15)$$

where  $T_m$  is the annual mean temperature of deep soil ( $^{\circ}\text{C}$ ),  $T_{amp}$  is the annual amplitude of surface temperature ( $^{\circ}\text{C}$ ),  $t_0$  is the time lag from a starting date to the occurrence of the minimum temperature in a year and  $D$  is the damping depth (m) of annual fluctuation,

$$D = \sqrt{\frac{365}{\pi} \frac{86400k}{\rho C}} .$$

The initial soil moisture content is assumed to be uniform in the absence of its variation pattern at a specific time.

## 2.3 Boundary Conditions

Boundary conditions include heat and moisture transfer for the ground or top soil surface, the bottom face and four vertical faces as well as the inlet and outlet openings and the interior and exterior surfaces of the heat exchanger pipe.

### 2.3.1 Soil surface

Boundary conditions for heat transfer through the soil surface include the ambient and soil surface conditions for radiation, convection and evaporation/condensation heat transfer as well as sensible heat transfer due to precipitation. For a top control volume of unit cross section and  $\delta\xi$  thickness normal to the soil surface, assuming that heat and mass transfer occurs in one direction only, the energy balance requires that

$$\left(k + L\rho_l D_{T,v}\right) \frac{\partial T}{\partial \xi} + L\rho_l D_{\Theta,v} \frac{\partial \Theta}{\partial \xi} = \pm q_r \pm q_c \pm q_e \pm q_p \quad (16)$$

where  $\xi$  is the direction normal to the surface. The terms on the right hand side represent the net heat flow due to radiation, convection, evaporation/condensation and precipitation into the control volume.

The radiation heat transfer ( $q_r$ ) includes short wave radiation from solar radiation ( $q_{rs}$ ) and long wave radiation between the soil surface and ambient environment ( $q_{rl}$ ). The solar radiation consists of direct (beam) radiation and diffuse radiation which can be obtained from a local weather station. Analytical expressions such as sinusoidal one for daily cyclic variations can be used to represent the direct solar radiation but this is less accurate for the diffuse radiation. As the diffuse radiation could be as much as one half of the total radiation in the UK at times, data from statistic weather files are used rather than an analytical expression to represent the incident solar radiation.

The long wave radiation is given by

$$q_{rl} = \sigma \varepsilon (T_s^4 - T_{sky}^4) \quad (17)$$

where  $\sigma$  is the Stefan-Boltzmann constant ( $= 5.67 \times 10^{-8} \text{ W/m}^2\text{K}^4$ ),  $\varepsilon$  is the emissivity of soil surface or ground cover,  $T_s$  is the temperature of soil surface or ground cover (K) and  $T_{sky}$  is the sky temperature (K) .

The sky temperature is related to the air temperature and cloud cover [32]:

$$T_{\text{sky}} = 9.365574 \times 10^{-6} (1-cc) T_a^6 + cc [(1-0.84 cc) (0.527 + 0.161 e^{8.45(1-273.15/T_a)}) + 0.84 cc] T_a^4 \quad (18)$$

where  $T_a$  is the air temperature (K) and  $cc$  is the cloud cover (in fraction of 1).

The air temperature, like other meteorological data, can be obtained from a weather station. Alternatively the air temperature at any hour of a day in a year can be represented by

$$T_a = T_{\text{max}} - \frac{T_{\text{max}} - T_{\text{min}}}{2} \left[ 1 - \sin\left(\frac{(t-9)\pi}{12}\right) \right] \quad (19)$$

where  $T_{\text{min}}$  and  $T_{\text{max}}$  are the minimum and maximum temperatures (K) of air in a month.

The convective heat transfer between the soil surface and ambient air ( $q_c$ ) results from combined wind and buoyancy effects and is dependent on the soil surface temperature, ambient temperature, local wind speed and vegetation height [33].

The latent heat transfer due to evaporation of water vapour from the soil surface (or moisture condensation to the soil surface) is given by

$$q_e = L (\rho_s - \rho_a)/(r_s + r_a) \quad (20)$$

where  $\rho_a$  and  $\rho_s$  are the densities of water vapour in air and soil surface, respectively, ( $\text{kg/m}^3$ );  $r_a$  and  $r_s$  are the resistances to vapour transfer by air and by the soil surface (or stamamol of plant), respectively, (s/m).

The resistance of air is the inverse of the mass diffusivity of water vapour and the resistance of the soil surface is related to the moisture content by the following expression [34]:

$$r_s = 33.5 + 3.5 (\Theta_s/\Theta)^{2.3} \quad (21)$$

The sensible heat transfer due to precipitation ( $q_p$ ) during a time step is calculated from the amount of rainfall that is absorbed by the top control volume of soil up to saturation while excess rainwater is assumed to run off:

$$q_p = V_r \rho_r C_r (T_{\text{wb}} - T_s) \quad (22)$$

where  $V_r$  is the rainfall ( $\text{m}^3/\text{s}$ );  $\rho_r$  and  $C_r$  are the density ( $\text{kg/m}^3$ ) and specific heat ( $\text{J/kgK}$ ) of rainwater, respectively; and  $T_{\text{wb}}$  is the wet bulb temperature of air (K).

Climatic data is generally based on statistics but, unlike solar radiation and other weather information, detailed distribution of rainfall within a day is not readily available. Therefore, the equivalent rate of rainfall is calculated from the monthly rainfall and the duration of rain. As an independent parameter, the sensible heat transfer could theoretically be calculated for the whole day with cloud cover as an indicator the average of which during sunshine time (2.49 oktas = 31.1%) is very close to the proportion of rain days in a year (111 days or 30.4%) for southern England [35]. However, this would cover the time when the sun shines for the calculation of radiation and evaporation heat transfer. Therefore, precipitation is assumed to occur every third day during the evening hours between 20:00 and 23:00 when the air temperature is also close to the daily average value.

The boundary condition for moisture transfer at the soil surface is given by the moisture balance, similar to the heat balance:

$$(D_{T,l} + D_{T,v}) \frac{\partial T}{\partial \xi} + (D_{\Theta,l} + D_{\Theta,v}) \frac{\partial \Theta}{\partial \xi} = V_p \pm V_e \quad (23)$$

The terms on the right hand side represent the net flow of moisture due to precipitation and evaporation/condensation into the control volume of unit cross section and  $\delta\xi$  thickness. The upper limit of moisture in soil is the saturation moisture content and the lower limit is the residual moisture content. The moisture decrease in soil due to evaporation or increase resulting from precipitation or condensation at any time is set within these lower and upper limits.

### 2.3.2 Vertical faces and bottom face for soil

Equation 15 is used for specifying the soil temperature at the bottom face and two vertical faces in parallel with the direction of heat exchanger pipe. For the other two vertical edges normal to the pipe flow direction, zero heat flux is imposed. For moisture transfer, the mass flux is set to zero for all these faces.

### 2.3.3 Inlet and outlet openings of heat exchanger pipe

The boundary conditions for the pipe inlet are set the same as those for the ambient, i.e., air temperature and vapour pressure (or relative humidity) for a given ventilation rate (or velocity). The moisture content of inlet air is calculated from these conditions. For the pipe outlet, the heat and mass fluxes are set to zero.

### 2.3.4 Interior surface of heat exchanger pipe

The boundary condition for heat transfer inside the pipe of constant diameter is based on the heat balance of moist air in a finite section  $d\eta$  of the pipe:

$$\frac{\partial(\rho_f C_f T_f)}{\partial t} = \frac{\partial}{\partial \eta} \left( -\rho_f C_f V T_f + k_f \frac{\partial T_f}{\partial \eta} \right) + \frac{4}{d_i} h_f (T_f - T_{pi}) + \frac{4}{d_i} L h_m (\rho_v - \rho_{vp}) \quad (24)$$

where the left hand side represents heat accumulation in moist air. The terms on the right hand side are the advective and conductive heat gain of the air through a finite section of  $d\eta$  (in flow direction), convection heat transfer between pipe and air, and the condensation (or subsequent evaporation if the condensate is not drained away) heat transfer, respectively;  $\rho_f$ ,  $C_f$  and  $k_f$  are the density ( $\text{kg/m}^3$ ), specific heat ( $\text{J/kgK}$ ) and thermal conductivity ( $\text{W/mK}$ ) of moist air, respectively;  $T_f$  and  $T_{pi}$  are the temperatures of moist air and interior surface of pipe, respectively, (K);  $V$  is the mean velocity of air in the pipe (m/s);  $d_i$  is the inner diameter of pipe (m);  $h_f$  is the convection heat transfer coefficient ( $\text{W/m}^2\text{K}$ );  $h_m$  is the mass convection coefficient (m/s);  $\rho_{vp}$  is the density of water vapour at pipe surface temperature ( $\text{kg/m}^3$ ).

The heat transfer coefficient for the forced convection between the internal pipe surface and supply air is [36]:

$$h_f = \frac{k_f f}{d_i} \frac{(\text{Re}-1000) \text{Pr}}{8 \left[ 1 - 12.7 \sqrt{f/8} (\text{Pr}^{2/3} - 1) \right]} \quad (25)$$

where Re is the Reynolds number, Pr is the Prandtl number and f is the friction factor,  $f = [0.79 \ln(\text{Re}) - 1.64]^{-2}$ .

The boundary condition for moisture transfer at the interior surface of the pipe is based on the mass balance of water vapour in supply air in one-dimensional flow along the pipe:

$$\frac{\partial \Theta}{\partial t} = \frac{\partial}{\partial \eta} \left( -V\Theta + D_v \frac{\partial \Theta}{\partial \eta} \right) + \frac{4h_m}{d_i} \left( \Theta - \frac{\rho_{vp}}{\rho_l} \right) \quad (26)$$

The last term on the right hand side represents the rate of moisture transfer due to condensation or evaporation.

When preheating or cooling of incoming air is not suitable (at times when air temperature is higher than the pipe temperature for heating demand or lower than the pipe temperature for cooling), zero heat and mass fluxes are specified as the boundary condition for the pipe surface, together with zero ventilation rate (velocity) at the inlet opening.

### 2.3.5 Exterior surface of heat exchanger pipe

The heat transfer at the interface between soil and the pipe surface is calculated using the general heat transfer equation, assuming that there is no contact resistance.

It is assumed that the pipe wall is impervious to fluid flow. Then, the boundary condition for moisture transfer at the interface between soil and the impermeable pipe surface is

$$\left(D_{T,l} + D_{T,v}\right)\frac{\partial T}{\partial \xi} + \left(D_{\Theta,l} + D_{\Theta,v}\right)\frac{\partial \Theta}{\partial \xi} = 0 \quad (27)$$

## **2.4 Validation**

The accuracy of the in-house program was examined for heat transfer by comparison with a commercial program FLUENT [37] which had been validated for simulation of ground-coupled heat exchangers [38]. The heat transfer was modelled through a straight pipe of 200 mm external diameter buried 1.5 m below the ground for a fixed ambient air temperature of 5°C and a soil mixture with constant properties and an initial and deep temperature of 10°C. Detailed conditions for validation are shown in Fig. 3. The soil properties were taken from the measurement at a site in Southern England where the performance of a ground-coupled heat pump was monitored. The measured soil density, specific heat and thermal conductivity were 1588 kg/m<sup>3</sup>, 1465 J/kgK and 1.24 W/mK, respectively [38]. The calculated heat transfer coefficient for the soil surface resulting from both buoyancy and wind effects was 17.4 W/m<sup>2</sup>K for soil at a temperature of 10°C and air at a temperature of 5°C and speed of 4 m/s (the annual mean wind speed in the area) while the coefficient for forced convection inside the pipe was equal to 8.7 W/m<sup>2</sup>K based on Equation (25) for an air velocity of 2 m/s and temperature of 1°C. In order to compare the results from the two programs, transient heat transfer simulation was first carried out using the in-house program where time steps had been optimised for different periods of operation, ie a time step of one second for the first hour and gradually increasing to five minutes after 10 days, and where equations for the calculation of heat transfer coefficient were included. The same values of boundary conditions including the calculated heat transfer coefficient and time steps were then used in FLUENT for simulation. The main results from the two sets of simulation include temperature and heat flux distributions in the computational domain at different times and the history of heat flux or heat transfer rate through the boundary. The most important parameter for assessing the thermal performance of a ground-coupled heat exchanger is the amount and rate of heat transfer through the heat exchanger. Fig. 4 shows the predicted heat transfer rate per unit length of the heat exchanger using the two programs. The results from the two programs agree very well with the differences of less than 1% during a period of 30 days. The difference between the simulation results increases from about 0.1% in the first hour to a maximum of just under 0.6% at about 15 hours. The difference then decreases with time to under 0.2% at Day 5 and diminishes after 20 days.

For accurate simulation of heat and moisture transfer, cells (control volumes) should be sufficiently small near the sources of heat and moisture transport such as the soil surface and heat exchanger. To avoid the need for an excessively large mesh size, a non-uniform mesh is therefore used with dense cells allocated near the heat exchanger and soil surface.

The effect of mesh size is illustrated in Fig. 5 through a comparison of the predicted heat transfer rate using different mesh sizes (in terms of edge size normal to pipe surfaces) near a 200 mm pipe installed 1.5 m below the ground for two sets of conditions – one for a constant air temperature of 5°C and initial soil temperature at 10°C and the other with varying soil and environmental conditions for October in Southern England as described in Section 3. The difference is expressed as the ratio of the change in the heat transfer from a smaller mesh size to a larger size; eg, the ratio for mesh sizes between 10 mm and 5 mm is equal to (value for 5 mm – value for 10 mm)/(value for 5 mm) and is represented by a line with a legend 10mm/5mm. It is seen that under constant conditions increasing the mesh size would under predict the heat transfer through the pipe and the difference or error in the predicted heat transfer decreases with increasing time. Overall the effect of mesh size is not significant for predicting a long period of operation. With smaller mesh sizes the difference diminishes after 2 days' operation and even with larger mesh sizes it is less than 0.5% at the end of 5 days. However, for realistic and varying soil and environmental conditions, the difference in the predicted heat transfer using different mesh sizes would partly accumulate and thus increase with time. The difference between the mesh sizes of 1.25 and 2.5 mm stabilises at 1.5% after about 10 days' operation but it would take about 30 days for the difference between predictions with larger mesh sizes to reach a constant of over 3%. Also, increasing the mesh size would under predict the heat transfer only at the beginning (for about 0.5 hour) but over predict it afterwards. The predicted heat transfer using a 10 mm mesh size would be over 8% larger than that using a 1.25 mm size at the end of 30 days. Therefore, for accurate dynamic simulation of long term operation, the mesh size near the heat exchanger pipe should be around 1 mm or less. The edge size of the cells near the heat exchanger and the soil surface used in this study is about 1 mm, increasing gradually to a maximum of 25 mm at the bottom or vertical faces of the domain. In order to simulate accurately the transient state heat and moisture transfer through a horizontally coupled ground heat exchanger, the time step should also be sufficiently small to capture the rapid temperature/moisture changes, e.g., at the beginning of continuous operation, or switch-on and -off times of intermittent operation, or changeover times of operation modes between heating/cooling and recovery. For heat transfer alone, for instance, a too large time step from the beginning can lead to under prediction of the pipe surface temperature change and heat extraction rate [33 and 39].

### 3 RESULTS AND DISCUSSION

The computer program is used to simulate transient state heat and moisture transfer through an EAHX system for preheating and cooling of supply air in the Southern England climatic conditions. The following conditions and assumptions are utilised for the simulation: The heat exchanger is made of high density polyethylene with an external diameter of 200 mm and a wall thickness of 7.7 mm and is installed horizontally at 1.5 m below the ground surface. The hourly climatic conditions for each month including air temperature, partial vapour pressure (or wet bulb temperature), solar radiation, cloud cover, and wind speed are given by the CIBSE Guide J [40]. The monthly rainfall is based on the UK climate data [35]. Values at any time of a day are then calculated from these hourly/monthly climate data through linear interpolation. The mean velocity of incoming air at the inlet of the heat exchanger is 2 m/s. The soil is of loam texture with 43% sand, 18% clay and 39% silt [41]. Its saturation moisture content is 44% and residual moisture content 5%. The initial moisture content is taken to be one half of the saturation value. The temperature of deep soil ( $T_m$  in Equation 15) is 10°C. The vegetation height is 0.1 m, which is required for assessing wind-driven natural convection.

Fig. 6 shows the predicted daily variations in ambient air temperature, soil surface temperature and moisture, and mean moisture for the soil layer up to a depth between the soil surface and the crown of the pipe for heating in October. The daily air temperature varies by about 9°C from the minimum of 7.1°C in the early morning (3 am) to the maximum of 16.1°C in the afternoon (3 pm) at the beginning of the month. The air temperature drops gradually with the minimum and maximum to 5°C and 12°C, respectively, at the end of the month. The daily variation of soil surface temperature is much larger mainly because of absorption of solar radiation during the day and long wave radiation heat loss during the night. The daily soil temperature swing would have been even larger if not attenuated by moisture evaporation and natural convection. The minimum and maximum surface temperatures are about 3.9°C and 25.4°C, respectively, at the beginning of the month and decrease to 1.7°C and 20°C, respectively, at the end of the month. The surface moisture would drop rapidly after the sun rises and reach the minimum (residual) value at about 11 am, or 2pm if it rains in the night before, and would remain so till sunset because the evaporation rate would be larger than the moisture transfer rate from soil below. During the evening and onwards, the surface moisture would increase as a result of upward moisture transfer in soil and potential surface condensation if the temperature drops below the dew point. The mean moisture for the soil layer would increase during the rain on every third evening and then decrease afterwards. Overall, the amount of rainfall exceeds that of surface evaporation during the month. This is indicated by the higher mean moisture from Day 4 than the initial value; the lowest mean is 25.8% on day 6 before the next round of rain and 29.9% near the end of the month. It should be noted that, after the rain in the night before, the peak soil surface temperature on the following day would be lower than those for two days before and after due to the lower rainwater temperature (= wet bulb air temperature) and increased moisture evaporation.

The variations of soil temperature and moisture along a vertical line through the mid-length and centerline of the heat exchanger are shown in Fig. 7. The vertical soil temperature variation is influenced by the heat exchanger in an area of only 0.2 m from the pipe at the end of the first day. At night, the soil temperature decreases from heat transfer to the cold ambient at the top ground surface and heat extraction by the air in the heat exchanger (lower temperature at the pipe position). Due to the heat extraction, the average temperature of soil above the heat exchanger would decrease approaching the mean temperature of deep soil on Day 20 but the soil temperature below the heat exchanger would still be above the deep soil temperature. At the end of the month, the soil temperature above the heat exchanger would be lower than the deep soil temperature. While the soil temperature in the area between the heat exchanger and 2.5 m below is decreasing, the temperature of soil further below is increasing slightly due to the heat transfer from above (but still lower than the temperature of soil above).

Moisture evaporates from the soil during day times and it could condense to the soil surface during night times but the moisture variation at the end of the first day is limited to the close vicinity of soil surface. Condensation of moisture on the soil surface occurs as seen from the rise in the moisture content in the first night. The rainfall on the third day enables the moisture to increase in soil and the increase reaches the position of the heat exchanger after two days (five days from the start time). The peak soil moisture one day after rain (eg Day 10) is higher than that two days later (eg Day 20) but the mean soil moisture on Day 20 would be higher than that on Day 10 as some of the moisture would transfer to the soil around and below the heat exchanger. During the times with clear or overcast days and nights, the soil moisture increases with depth depending on the time lapse after rain, eg, about 0.46 m deep on Day 5 (two days after rain) and 0.39 m on Day 10 (one day after rain). However, the trend of soil moisture variation with depth would reverse with the maximum at the soil surface right after

rain as indicated for the variation at midnight after the evening rain (Day 30). Also, the influence of moisture variation reaches 3.5 m below the soil surface at the end of the month. It should be pointed out that the volumetric moisture content of air inside the heat exchanger ( $= 6 \text{ to } 8 \times 10^{-6}$ ) is negligible compared with the magnitude of soil moisture.

Fig. 8 shows the predicted variations with time in the temperature of the inner pipe surface and heat transfer rate for the first meter of horizontal section from the pipe inlet, as well as the ambient air temperature and the temperature of undisturbed soil at a depth of 1.5 m (denoted by soil temp) for reference, using the heat exchanger for heating in October. The temperature of the undisturbed soil at 1.5 m deep is about  $14.1^{\circ}\text{C}$  at the beginning of the month and decreases to  $12.6^{\circ}\text{C}$  at the end of the month. It is higher than the night time air temperature.

The temperature of the heat exchanger (inner pipe surface temperature) also varies rapidly during the first few minutes of each session of heating operation. For the first day as an example, it takes about 6 minutes for the temperature of the heat exchanger to drop from  $14.1^{\circ}\text{C}$ , the initial equilibrium condition with soil at the installation depth, by 1 K to  $13.1^{\circ}\text{C}$  but takes about 1.4 more hours by another 1 K and 4.5 hours to reach the minimum of the day at  $11.5^{\circ}\text{C}$ .

The predicted heat transfer rate for the first meter pipe at start is at a maximum of  $24.3 \text{ W/m}$  when the temperature difference between the surrounding soil and incoming air is at maximum (Fig. 8). It decreases to zero in 10 hours as the air temperature rises much faster than the surrounding soil in the morning so that the air temperature reaches the internal pipe surface temperature by the time. After 10am, the air temperature is higher than the pipe temperature and heat would be transferred from air to soil if air were still forced through the pipe. During the evening, the air temperature drops below the pipe temperature at about 7pm and heat is transferred again from warmer soil to cooler air. The rate of heat transfer increases until at about 3am the following day and then decreases to zero again at 10am in the morning. The cycle of heat transfer repeats each day and the rate of heat transfer would decrease day by day due to the decreasing soil temperature. However, because air temperature is also decreasing, the change in the heat transfer rate would not be significant. For example, the maximum heat transfer rate would decrease from  $24.3 \text{ W/m}$  at the beginning to  $21.1 \text{ W/m}$  after one day's operation and to  $20.5 \text{ W/m}$  and  $20.4 \text{ W/m}$  at Day 5 and Day 10, respectively, but slightly increase to  $20.7$  and  $20.9 \text{ W/m}$  at Day 20 and Day 30, respectively. Note that the peak heat transfer rate for the first day starting at midnight is unusually high because of the large initial temperature difference between soil and air.

The temperatures of soil, air and heat exchanger and the heat transfer rate also vary along the air flow direction (inside the heat exchanger). The variations in the pipe and air temperatures and heat transfer rate are shown in Fig. 9 for a 40 m long heat exchanger at the end of Day 5. The air temperature increases along the heat exchanger as expected from  $7.8^{\circ}\text{C}$  at the inlet to  $12.7^{\circ}\text{C}$  at the outlet because of heat transfer from soil to air. The pipe temperature also increases along the heat exchanger from  $11.4^{\circ}\text{C}$  to  $13.4^{\circ}\text{C}$  because more heat transfer takes place near the entrance during the day and before. The increase in the pipe temperature is smaller than that in the air temperature along the air passage and thus the temperature difference between the pipe and air (heating potential) is much larger near the entrance. For example, the heat transfer rate decreases along the pipe by five times from  $17.9 \text{ W/m}$  at the inlet to  $3.2 \text{ W/m}$  at the outlet. It can be observed that the changes in the temperatures and heat transfer rate along the pipe are not linear. The heat transfer rate of the EAHX at the end of Day

5 can be approximately represented by the following quadratic correlation (though a cubic correlation would be nearly perfect),

$$q = 0.007728 x^2 - 0.6588 x + 17.54 \quad (R^2 = 0.9985) \quad (28)$$

where  $q$  is the heat transfer rate per unit length (W/m) and  $x$  is the horizontal distance from pipe inlet (m).

The following table from the quadratic regression shows that the p-value for each of the three terms in Equation (28) is close to 0. Hence, all three coefficients are significant for the correlation.

	Coefficients	Standard Error	t Stat	p-value	Lower 95%	Upper 95%
Intercept	1.754E+01	7.09E-02	2.47E+02	7.26E-75	1.74E+01	1.77E+01
x	-6.588E-01	8.19E-03	-8.05E+01	5.29E-52	-6.75E-01	-6.42E-01
x <sup>2</sup>	7.728E-03	1.98E-04	3.90E+01	1.90E-37	7.33E-03	8.13E-03

The heat transfer through the heat exchanger is highly influenced by the interactions between the pipe and surrounding soil together with ambient conditions that impact the operation of the system. Without consideration of these interactions, i.e., the soil temperature at pipe location is given by Equation 15 as used in some of the previous investigations [14-16], the predicted heat transfer rate would be much higher because of the much higher soil temperature and hence pipe temperature and the heat transfer rate would increase with time on a daily basis because of fast decreasing air temperature and thus increasing temperature difference between soil (or pipe) and air. Fig. 10 shows that, without the cooling effect of supply air, the daily variation of interior pipe surface temperature and its decreasing rate with time are much less than those with thermal and moisture interactions between the pipe and soil. Consequently, the difference between the two temperature values with and without consideration of the interactions increases with operating time; eg, on the 5<sup>th</sup> day, the maximum difference reaches 22% in the heating period (night time and peak at around 5am) and the minimum difference is 9% at the end of the temperature recovery period (day time), and on the 15<sup>th</sup> day, the corresponding maximum and minimum differences increase to 33% and 17%, respectively. The difference in the heat transfer rate shown in Fig. 11 is larger than that in the temperature (in Fig. 10) and the peaks and troughs of its daily variation do not follow those of temperature variation. For example, at the end of the month, the minimum difference in the heat transfer rate is 91% compared with 32% for the temperature difference. The minimum difference in the heat transfer rate generally occurs at night between 1am and 2am. The difference would be much larger at other times particularly when the air temperature approaches the pipe temperature, leading to negligible heat transfer, during the evening and early morning and hence there would be no preheating in daytime for simulation with the interactions whereas simulation without considering the interactions would indicate as if heat could be extracted nearly all day long. The amount of daily heat extraction, which is the cumulative product of the heat transfer rate and time for the duration of heating period, increases with time even for the prediction with full consideration of the interactions because of the increase in the potential heating period as a result of faster decreasing air temperature than soil temperature. The difference in the daily heat extraction predicted with and without consideration of the interactions is even larger; for example, for the last day of the month, the predicted daily heat extraction without considering the interactions is 178% higher than that with full interactions.

The degree of the impact of the interactions also varies along the air flow direction. As mentioned before, due to the interactions between the heat exchanger and the surrounding soil and atmosphere, air and pipe temperatures increase along the heat exchanger whereas the heat

transfer rate decreases. Without considering the interactions between the heat exchanger and the soil and ambient environments, the soil temperature at a given depth would theoretically be uniform. Consequently, the variation of pipe temperature along the heat exchanger is smaller but the variation in the air temperature is larger as the potential for heat transfer is larger near the air entrance which is indicated in Fig. 12 by the higher heat transfer rate without considering the interactions compared with the prediction with the interactions. By contrast, the decrease in the heat transfer rate along the heat exchanger is larger without considering the interactions. As a result, after air flows through the heat exchanger for about 20 m, the heating potential and heat transfer rate without considering the interactions become smaller than those with the interactions. However, the mean heat transfer rate for the whole pipe is still larger without considering the interactions ( $= 9.8 \text{ W/m}$ ) than that with the interactions ( $= 8.5 \text{ W/m}$ ) at the end of Day 5.

The heat transfer is also dependent on the length of the heat exchanger. The heat transfer and its rate per unit length decrease with increasing length as shown in Fig. 13 for the peak heat transfer rate ( $\text{W/m}$ ) and the amount of daily heat transfer ( $\text{Wh/m}$ ). The total heat transfer rate ( $\text{W}$ ) is the product of the mean heat transfer rate and the pipe length and this would however increase with length. As a result, the temperature of air flowing out of the heat exchanger would depend on the pipe length as well as the ambient air temperature. Fig. 14(a) shows that the increase in air temperature through a 1 m long pipe is negligible but a 10 m long pipe would be able to reduce the temperature difference between soil and ambient air or daily air temperature swing by  $1/3$ . The ambient air temperature is higher than the undisturbed soil temperature at the beginning of heating operation during much of the day time and hence preheating of supply air could be made use of only in the night time from sunset to sunrise. The (undisturbed) soil temperature appears to be much higher than air temperature in late October as if there were a potential for preheating all day long. This would have been the consequence if the interactions between the heat exchanger, soil and ambient environments were not taken into consideration. Without considering the interactions (Fig. 14(b)), a 10 m long pipe could have reduced the temperature difference between soil and ambient air or daily air temperature swing by  $1/2$  and a 40 m long could have maintained a nearly constant supply air temperature with a deviation from the soil temperature by only a degree or so (compared with a diurnal ambient air temperature swing of  $7^\circ\text{C}$ ). However, due to the interactions, the real soil temperature near the heat exchanger would decrease and the achievable supply air temperature would be lower. Hence, the error or the difference between the predictions with and without considering the interactions would increase with operating time as shown in Fig. 15 for a 40 m long heat exchanger. At the end of October, the difference in the predicted pipe temperature would be between 25% for the daytime and 34% for the night time. The corresponding difference in the supply air temperature would be from 21% to 28%. In other words, neglecting the interactions would over predict the air temperature rise through a 40 m long pipe by about  $1/4$ . The difference in the predicted heat transfer with and without considering the interactions would be even larger. Fig. 16 shows that the difference in the daily mean heat transfer rate (defined as the average heat transfer rate for the duration when heat is available for extraction) and daily heat transfer would reach 60% and 80%, respectively, at the end of one month's operation. The larger amount of daily heat transfer without considering the interactions results not only from the predicted higher heat transfer rate but also from the longer time period for heating of supply air – continuous heating from Day 14 due to faster decreasing ambient air temperature than soil temperature.

## 4 CONCLUSIONS

A computer program has been developed for the simulation of the dynamic thermal performance of earth-air heat exchangers for preheating and cooling of supply air. The effects of the heat exchanger length and dynamic interactions between the heat exchanger, soil and ambient environments have been investigated for heating operation. It has been found that the heat transfer rate and temperature rise of supply air per unit length decrease with increasing length of the heat exchanger but the overall amount of heat gain and temperature rise of supply air increase with the length. A heat exchanger of 0.2 m in diameter and 40 m in length would enable the supply air at a mean velocity of 2 m/s to be heated close to the soil temperature at the pipe location which differs from the temperature of undisturbed soil.

It has also been found that direct thermal and moisture interactions between the heat exchanger, soil and supply air have a significant impact on the heat transfer capacity. The predicted heat transfer rate decreases with increasing operating time. Neglecting the interactions would significantly over-predict the heat transfer rate and the amount of over-prediction increases with operating time. The results demonstrate that dynamic simulation using a validated three-dimensional numerical model would be required to provide accurate data for design or performance analysis of an earth-air ventilation system.

The computer program can be used for assessing the effects of various parameters on the performance of earth-air heat exchangers such as the thermal and physical properties of soil, heat exchanger size, installation depth and horizontal distance between parallel pipes and ventilation rate as well as the schedule/mode of operation. The program can also be used for predicting the dynamic thermal performance of hygroscopic building elements as well as ground-coupled heat exchangers for ground source heat pumps and for heat recovery from wastewater/sewer pipes, and distribution pipes for district heating/cooling.

## REFERENCES

- [1]. M.K. Ghosal, G.N. Tiwari, N.S.L. Srivastava, Thermal modeling of a greenhouse with an integrated earth to air heat exchanger: An experimental validation, *Energy and Buildings* 36 (2004) 219–227.
- [2]. M. Santamouris, G. Mihalakakou, C. Balaras, A. Argiriou, D. Asimakopoulos, M. Vallindras, Use of buried pipes for energy conservation in cooling of agricultural greenhouses, *Solar Energy* 55 (2) (1995) 111–124.
- [3]. C. Gauthier, M. Lacroix, H. Bernier, Numerical simulation of soil heat exchanger-storage systems for greenhouses, *Solar Energy* 60(6) (1997) 333–346.
- [4]. O. Ozgener, L. Ozgener, Determining the optimal design of a closed loop earth to air heat exchanger for greenhouse heating by using exergoeconomics, *Energy and Buildings* 43 (2011) 960–965.
- [5]. H. Breesch, A. Bossaer, A. Janssens, Passive cooling in a low-energy office building, *Solar Energy* 79 (2005) 682–696.
- [6]. F. Al-Ajmi, D.L. Loveday, V.I. Hanby, The cooling potential of earth–air heat exchangers for domestic buildings in a desert climate, *Building and Environment* 41 (2006) 235–244.
- [7]. J. Vaz, M.A. Sattler, E.D. dos Santos, L.A. Isoldi, Experimental and numerical analysis of an earth–air heat exchanger, *Energy and Buildings* 43 (2011) 2476–2482.

- [8]. L. Ramírez-Dávila, J. Xamán, J. Arce, G. Álvarez, I. Hernández-Pérez, Numerical study of earth-to-air heat exchanger for three different climates, *Energy and Buildings* 76 (2014) 238–248.
- [9]. R. Misra, V. Bansal, G.D. Agarwal, J. Mathur, T. Aseri, Thermal performance investigation of hybrid earth air tunnel heat exchanger, *Energy and Buildings* 49 (2012) 531–535.
- [10]. V. Bansal, R. Misra, G.D. Agrawal, J. Mathur, Performance evaluation and economic analysis of integrated earth–air–tunnel heat exchanger–evaporative cooling system, *Energy and Buildings* 55 (2012) 102–108.
- [11]. T. S. Bisoniya, A. Kumar, P. Baredar, Experimental and analytical studies of earth–air heat exchanger (EAHE) systems in India: A review, *Renewable and Sustainable Energy Reviews* 19(2013) 238–246.
- [12]. M.D. Paepe, A. Janssens, Thermo-hydraulic design of earth–air heat exchangers, *Energy and Buildings* 35 (2003) 89–97.
- [13]. K.H. Lee, R.K. Strand, The cooling and heating potential of an earth tube system in buildings, *Energy and Buildings* 40 (2007) 486–494.
- [14]. V.P. Kabashnikov, L.N. Danilevskii, V.P. Nekrasov, I.P. Vityaz, Analytical and numerical investigation of the characteristics of a soil heat exchanger for ventilation systems, *International Journal of Heat and Mass Transfer* 45 (2002) 2407–2418.
- [15]. F. Chlela, A. Husaunndee, P. Riederer and C. Inard, Numerical evaluation of earth to air heat exchangers and heat recovery ventilation systems, *International Journal of Ventilation* 6(1) (2007) 31–42.
- [16]. M. Krarti, J.F. Kreider, Analytical model for heat transfer in an underground air tunnel, *Energy Conversion and Management* 37(10) (1996) 1561–1574.
- [17]. R. Kumar, S. Ramesh, S.C. Kaushik, Performance evaluation and energy conservation potential of earth–air–tunnel system coupled with non-air-conditioned building, *Building and Environment* 38 (2003) 807–813.
- [18]. O.J. Svec, L.E. Goodrich, J.H.L. Palmer, Heat transfer characteristics of in-ground heat exchangers, *Energy Research* 7 (1983) 265–278.
- [19]. D. Deglin, L.V. Caenegem, P. Dehon, Subsoil heat exchangers for the air conditioning of livestock buildings, *Journal of Agriculture Engineering* 73 (1999) 179–188.
- [20]. P. Tittlein, G. Achard, E. Wurtz, Modelling earth-to-air heat exchanger behaviour with the convolutive response factors method, *Applied Energy* 86 (2009) 1683–1691
- [21]. R. Misra, V. Bansal, G.D. Agrawal, J. Mathur, T. Aseri, Transient analysis based determination of derating factor for earth air tunnel heat exchanger in summer, *Energy and Buildings* 58 (2013) 525–532.
- [22]. A. Tzaferis, D. Liparakis, M. Santamouris, A. Argiriou, Analysis of the accuracy and sensitivity of eight models to predict the performance of earth-to-air heat exchangers, *Energy and Buildings* 18 (1992) 35–43.
- [23]. P. Hollmuller, B. Lachal, Cooling and preheating with buried pipe systems: monitoring, simulation and economic aspects, *Energy and Buildings* 33 (2001) 509–518.
- [24]. C. Gauthier, M. Lacroix, H. Bernier, Numerical simulation of soil heat exchanger-storage systems for greenhouses, *Solar Energy* 60 (1997) 333–346.
- [25]. V.M. Puri, Heat and mass transfer analysis and modeling in unsaturated ground soils for buried tube systems, *Energy in Agriculture* 6 (1987) 179–193.
- [26]. G. Mihalakakou, M. Santamouris, D. Asimakopoulos, Modeling the thermal performance of the earth-to-air heat exchangers, *Solar Energy* 53 (1993) 301–305.

- [27]. J. Darkwa, G. Kokogiannakis, C.L. Magadzire, K. Yuan. Theoretical and practical evaluation of an earth-tube (E-tube) ventilation system, *Energy and Buildings* 43 (2011) 728–736.
- [28]. J. D. Campbell, Pore pressures and volume changes in unsaturated soils, PhD Thesis, University of Illinois at Urbana-Champaign, 1973.
- [29]. R.B. Clapp, G.M. Hornberger, Empirical equations for some soil hydraulic properties, *Water Resources Research* 14 (1977) 601-604.
- [30]. D.A. de Vries, Thermal properties of soils, in W.R. van Wijk (ed), *Physics of Plant Environment*, North-Holland Publishing Company, Amsterdam, 1963.
- [31]. S. Lu, T. Ren, Y. Gong, R. Horton, An improved model for predicting soil thermal conductivity from water content at room temperature, *Soil Science Society of America Journal* 71(2006) 8-14.
- [32]. R.J. Cole, The longwave radiation incident upon the external surface of buildings, *Building Services Engineers* 44 (1976) 195-206.
- [33]. G. Gan, Dynamic thermal modelling of horizontal ground source heat pumps, *International Journal of Low Carbon Technologies* 8(2) (2013) 95-105.
- [34]. S.F. Sun, Moisture and heat transport in a soil layer forced by atmospheric conditions, MSc Thesis, University of Connecticut, 1982.
- [35]. UK Climate, <http://www.metoffice.gov.uk/public/weather/climate/bracknell>. Accessed on April 5, 2013.
- [36]. V. Gnielinski, New equations for heat and mass transfer in turbulent pipe and channel flow, *Int. Chemical Engineering* 16 (1976) 359-368.
- [37]. ANSYS Inc. FLUENT, Canonsburg, Pennsylvania, 2010.
- [38]. Y. Wu, G. Gan, A. Verhoef, P.L. Vidale, R. Garcia Gonzalez, Experimental measurement and numerical simulation of horizontal-coupled slinky ground source heat exchangers, *Applied Thermal Engineering* 30(16) (2010) 2574-2583.
- [39]. G. Gan, CFD simulation for sustainable building design, in: R. Yao (ed), *Design and Management of Sustainable Built Environments*, Springer-Verlag, London, 2013, pp. 253-277.
- [40]. CIBSE, Guide J - Weather, solar and illuminance data, Chartered Institution of Building Services Engineers, London, 2002.
- [41]. B.J. Cosby, G.M. Hornberger, R.B. Clapp, T.R. Ginn, A statistical exploration of the relationships of soil moisture characteristics to the physical properties of soils, *Water Resources Research* 20(6) (1984) 682-690.

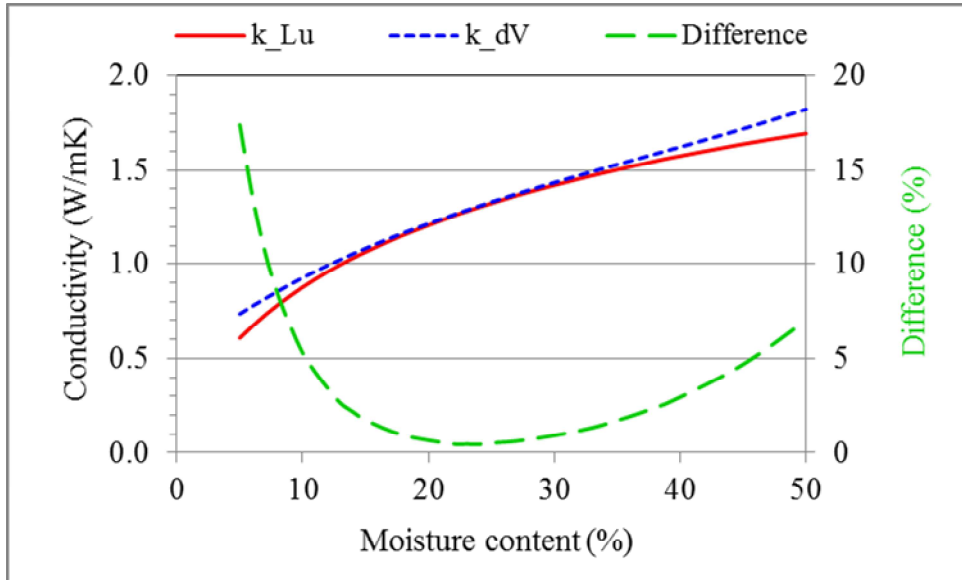


Fig. 1 Comparison of soil thermal conductivity using two methods

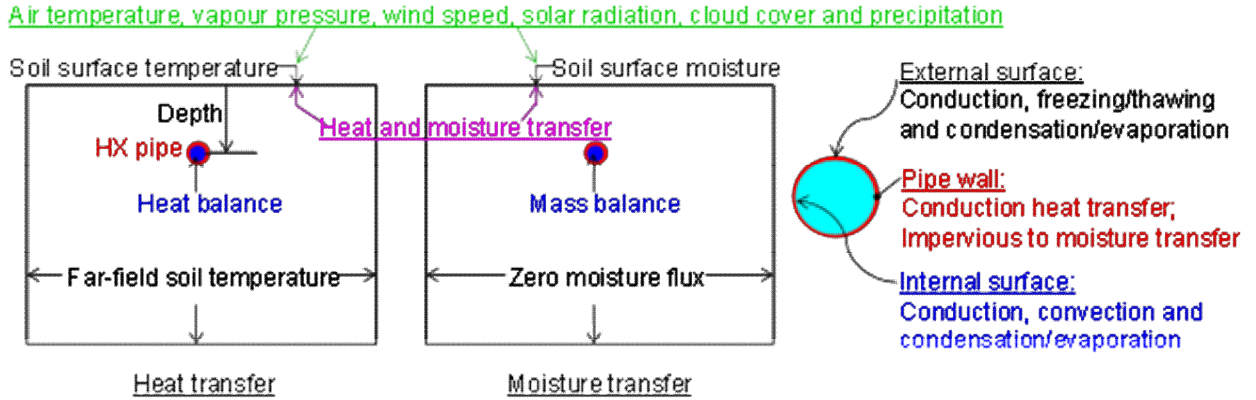


Fig. 2 Boundary conditions for simulation of heat and moisture transfer through an earth-air heat exchanger

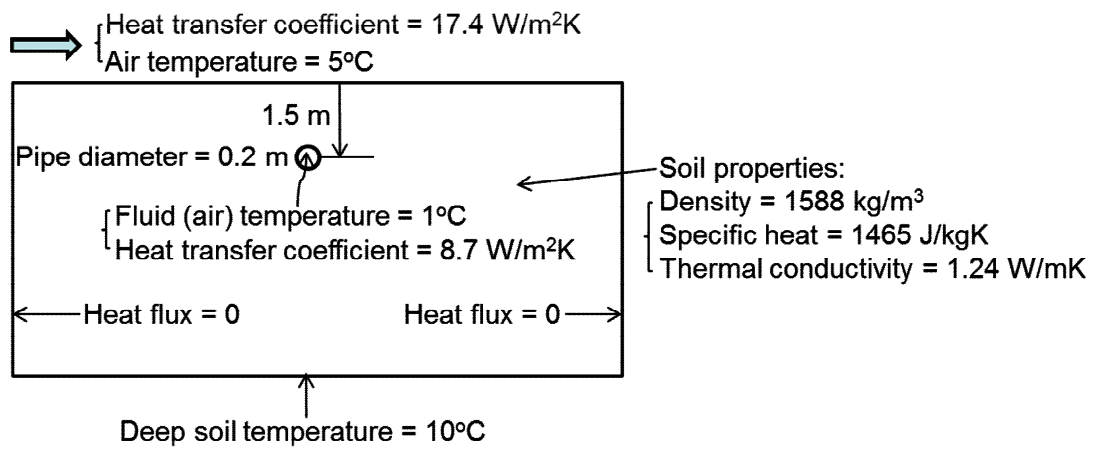


Fig. 3 Boundary conditions for validation

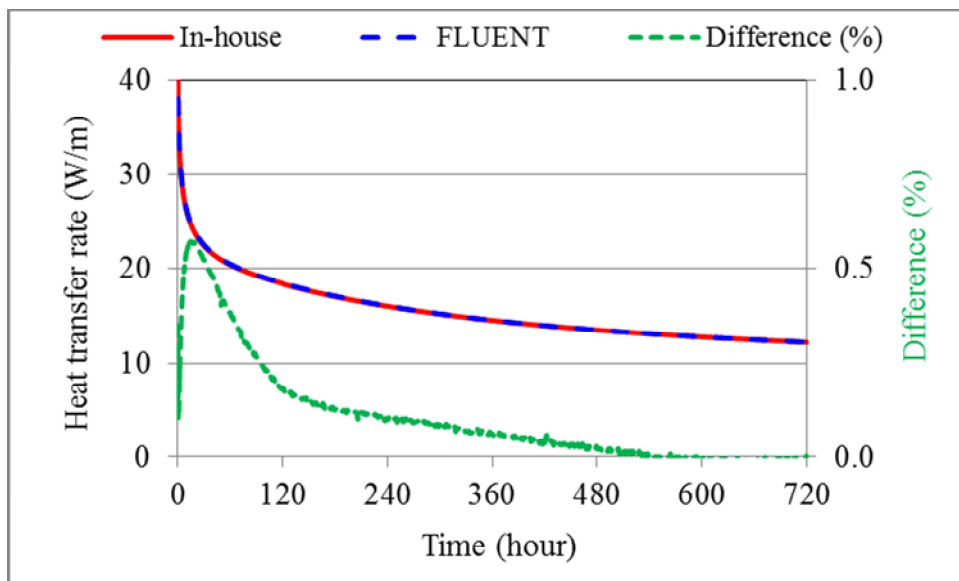
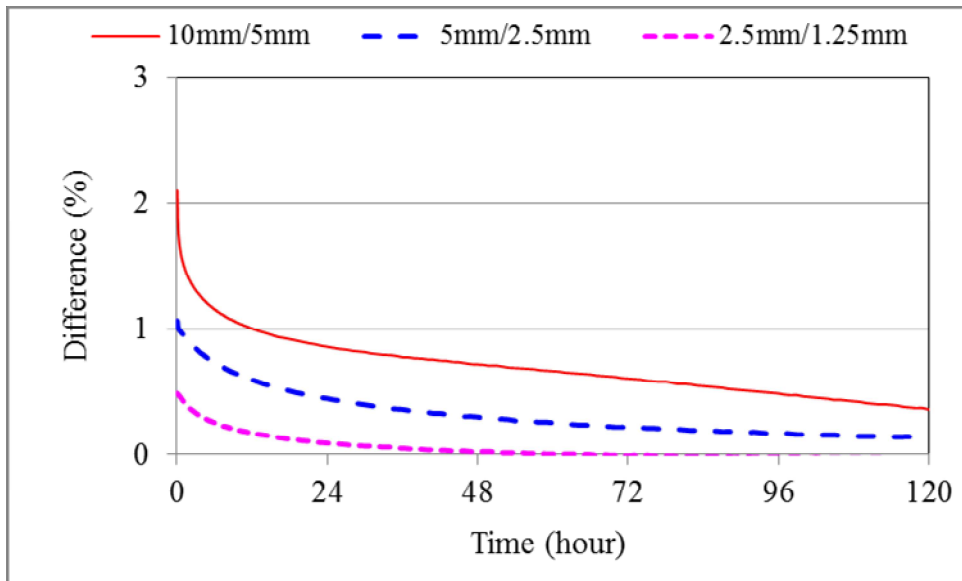
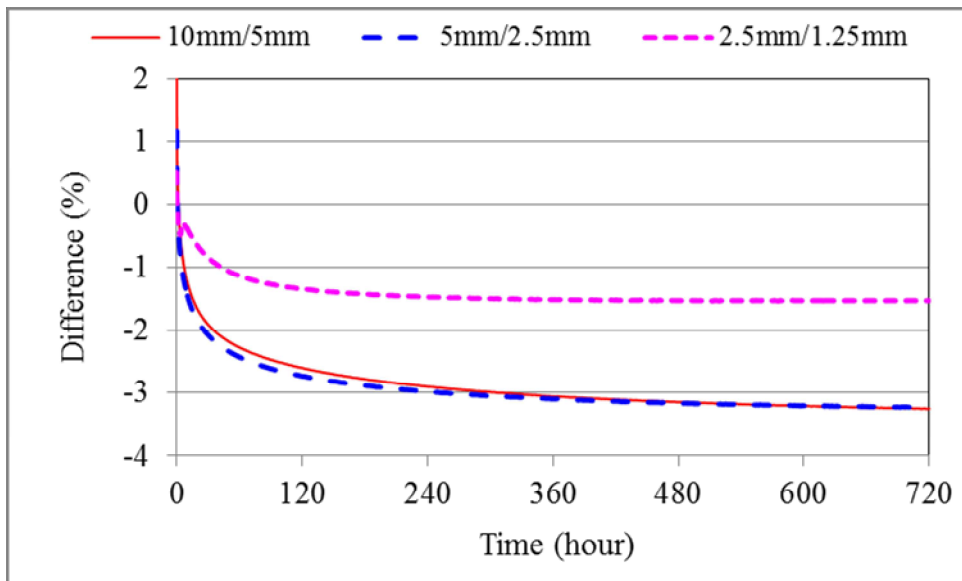


Fig. 4 Comparison of the predicted heat transfer rates using commercial and in-house programs

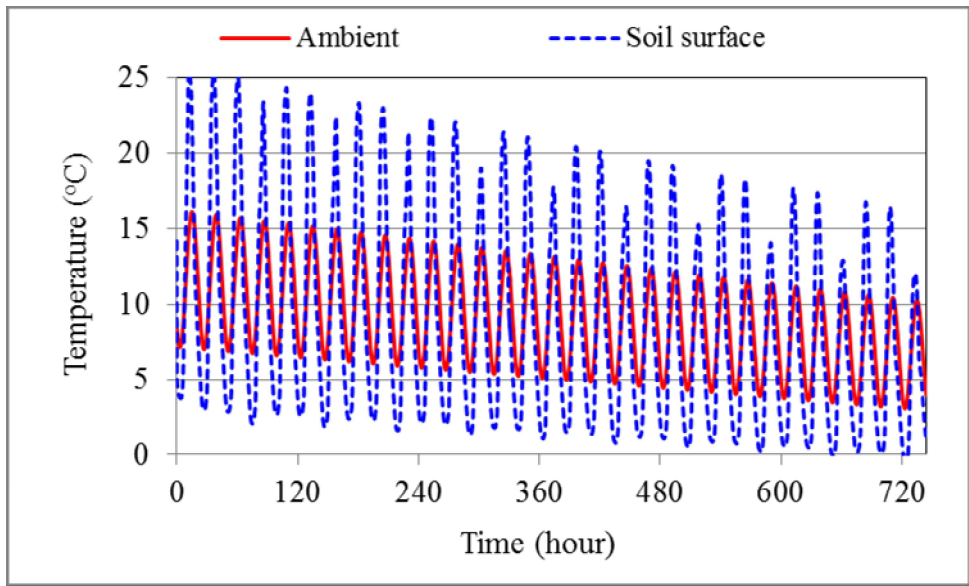


(a) Constant conditions

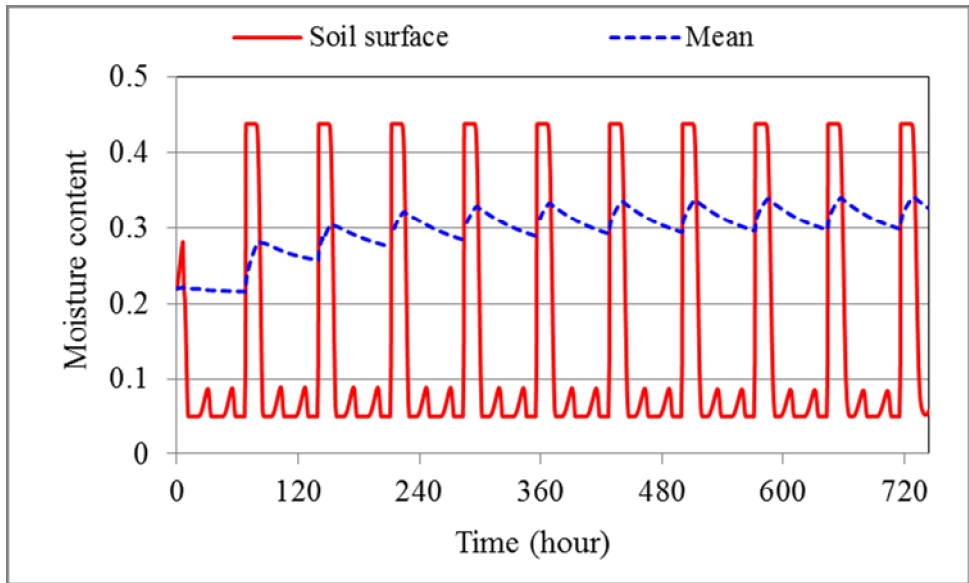


(b) Varying conditions

Fig. 5 Effect of mesh size on the predicted heat transfer rate

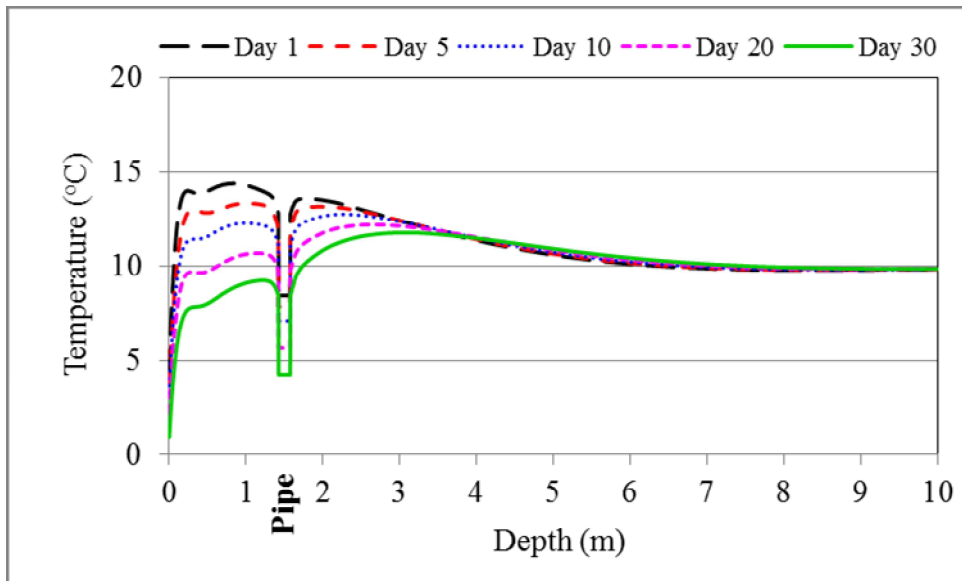


a) Temperature

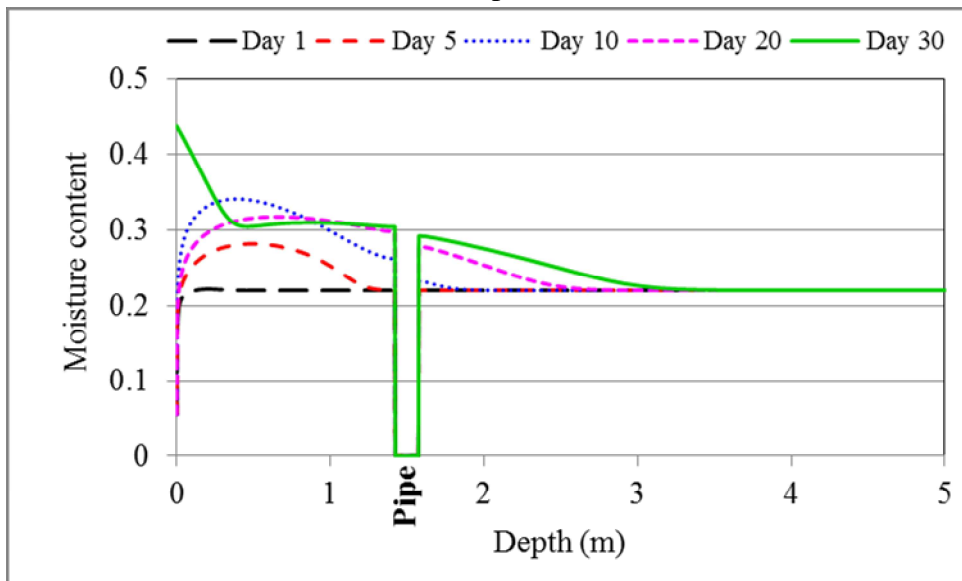


b) Moisture content

Fig. 6 Predicted daily variations in ambient air temperature, soil surface temperature and moisture, and mean soil moisture in October



a) Temperature



b) Moisture content

Fig. 7 Predicted vertical variations in soil temperature and moisture

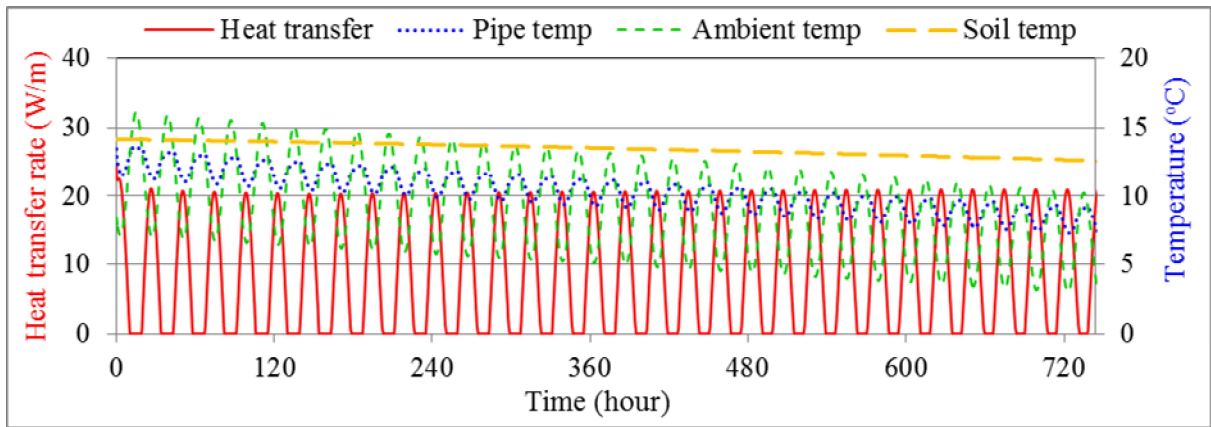


Fig. 8 Predicted variations with time of pipe temperature and heat transfer rate in October

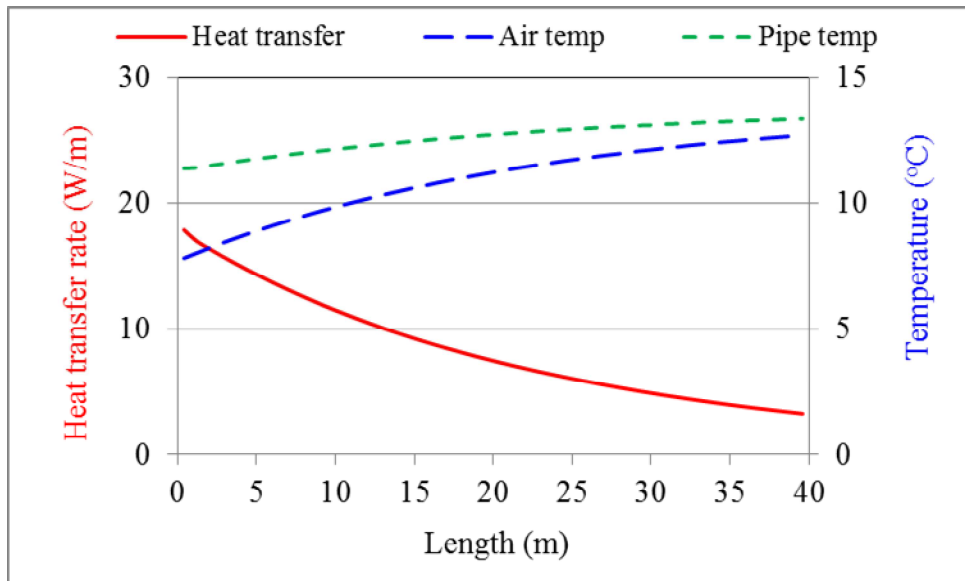


Fig. 9 Predicted variations with pipe length of supply air and pipe temperatures and heat transfer rate at the end of Day 5

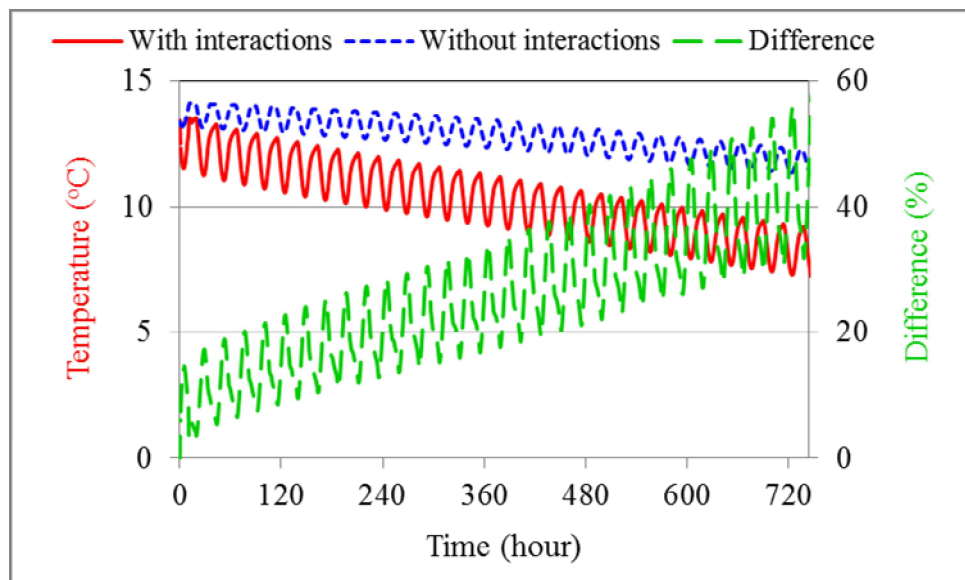
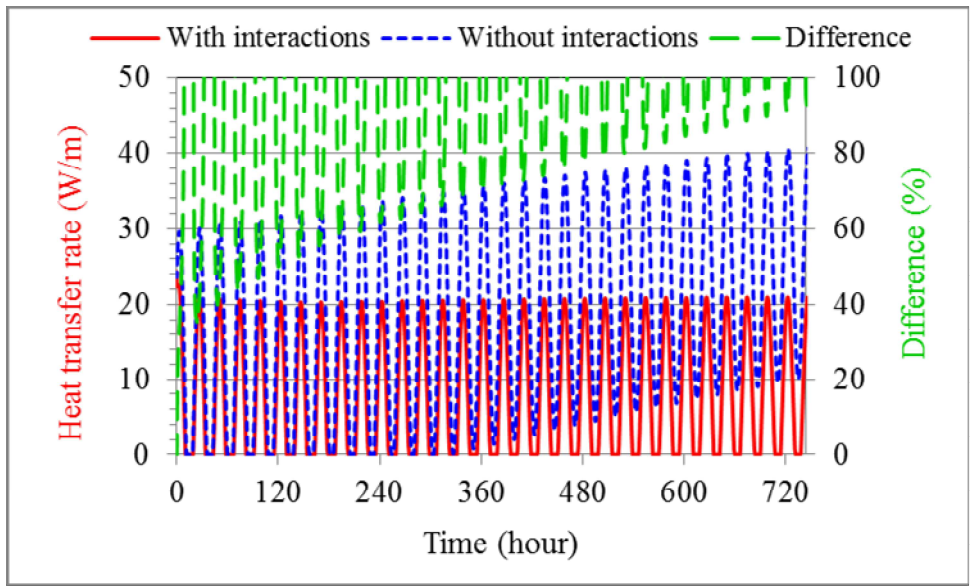
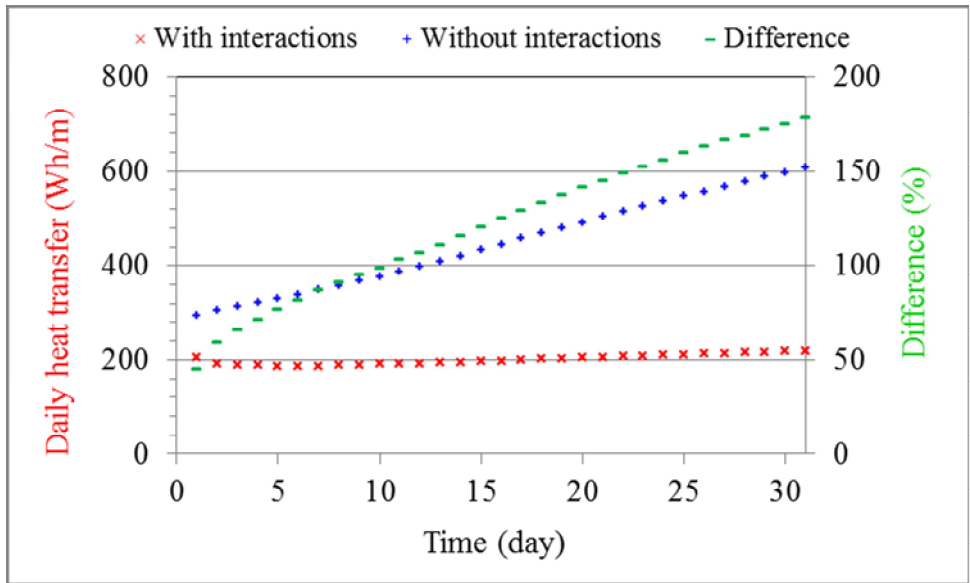


Fig. 10 Effect of interactions on the predicted variation in pipe temperature for the first meter of heat exchanger



(a) Heat transfer rate



(b) Daily heat transfer

Fig. 11 Effect of interactions on the predicted variation in heat transfer for the first meter of heat exchanger

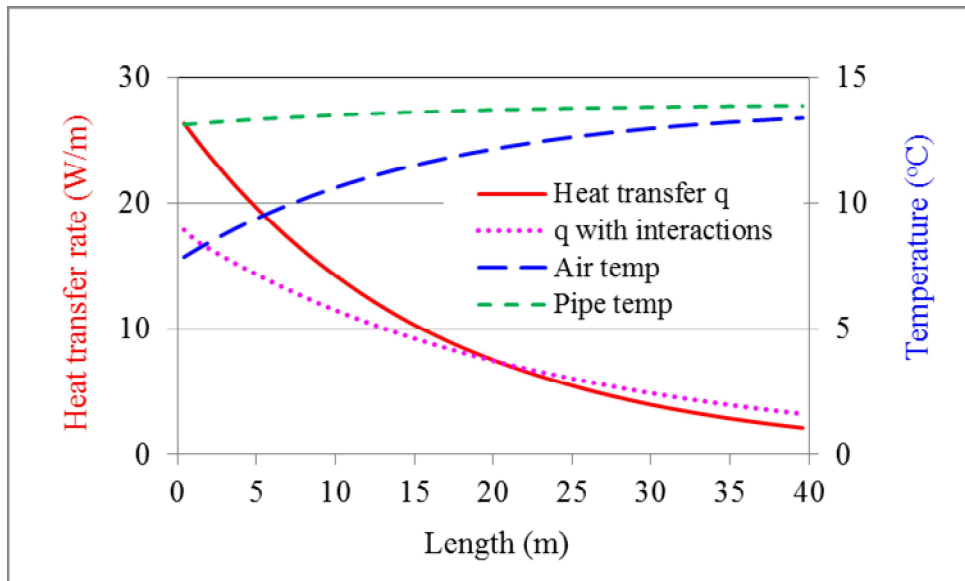
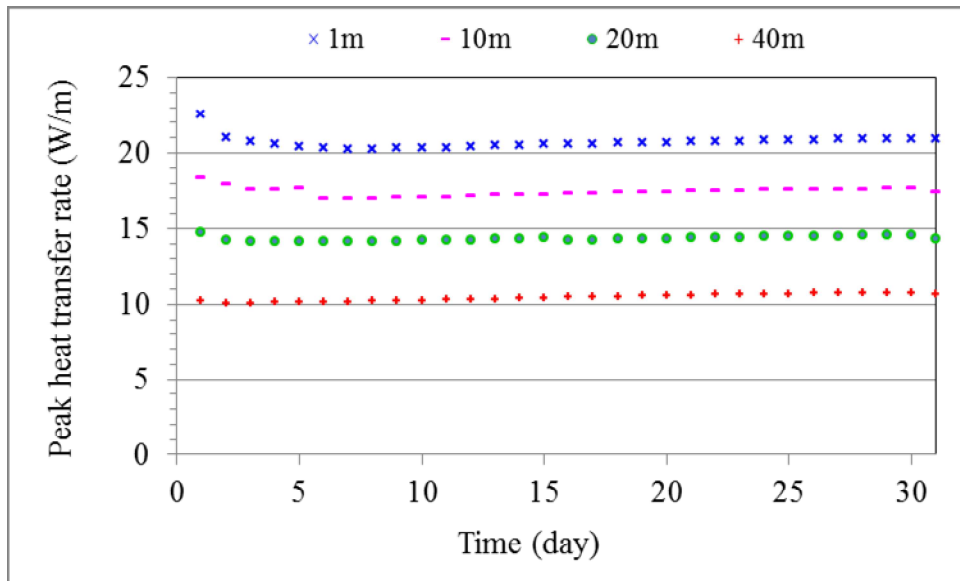
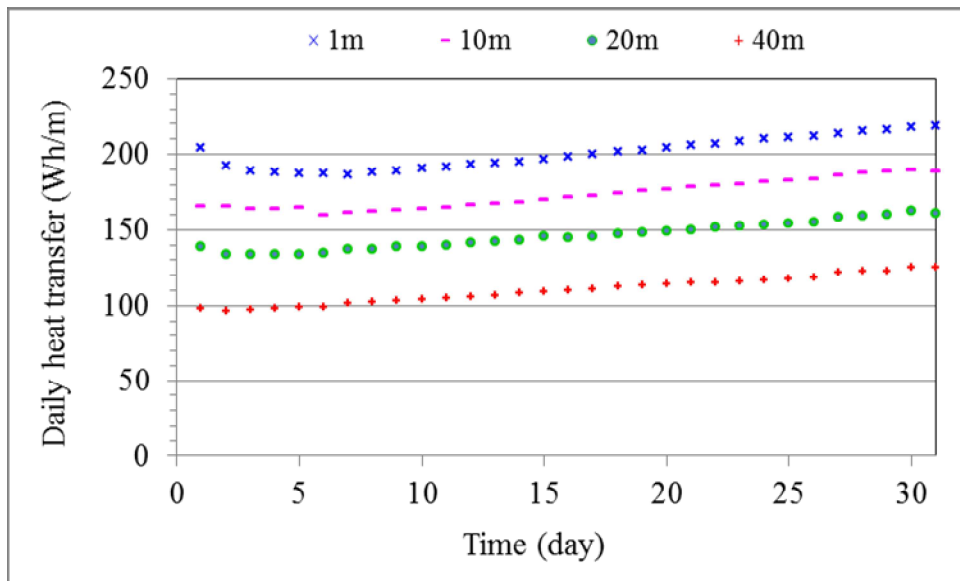


Fig. 12 Variations with pipe length of heat transfer rate and supply air and pipe temperatures at the end of Day 5 from the prediction without considering interactions

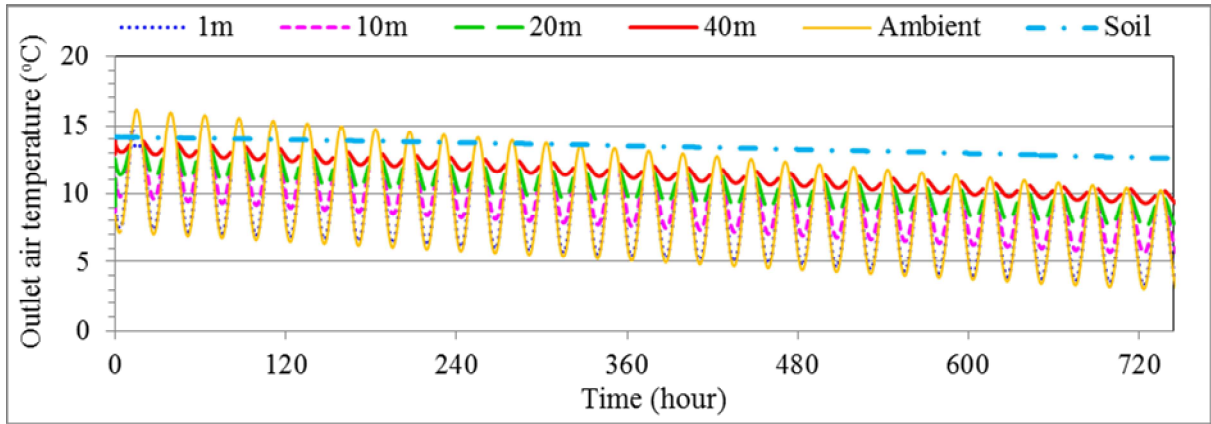


(a) Peak heat transfer rate

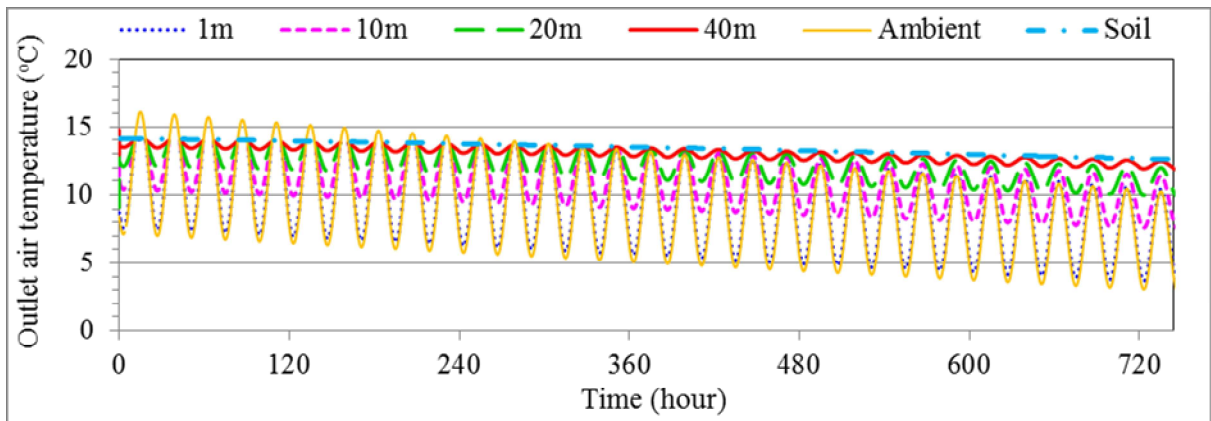


(b) Daily heat transfer

Fig. 13 Predicted variations of heat transfer with time for different heat exchanger lengths

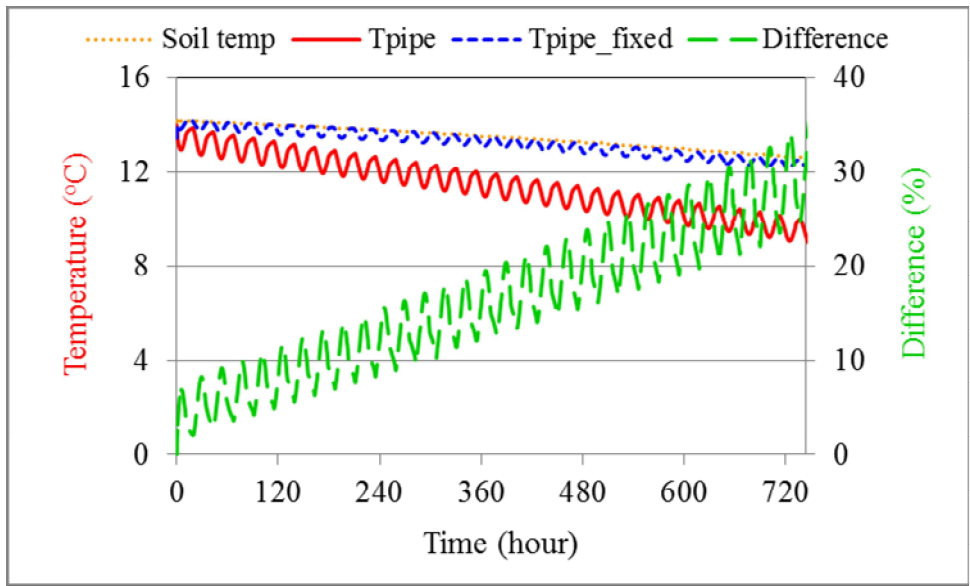


(a) With interactions between heat exchanger and environments

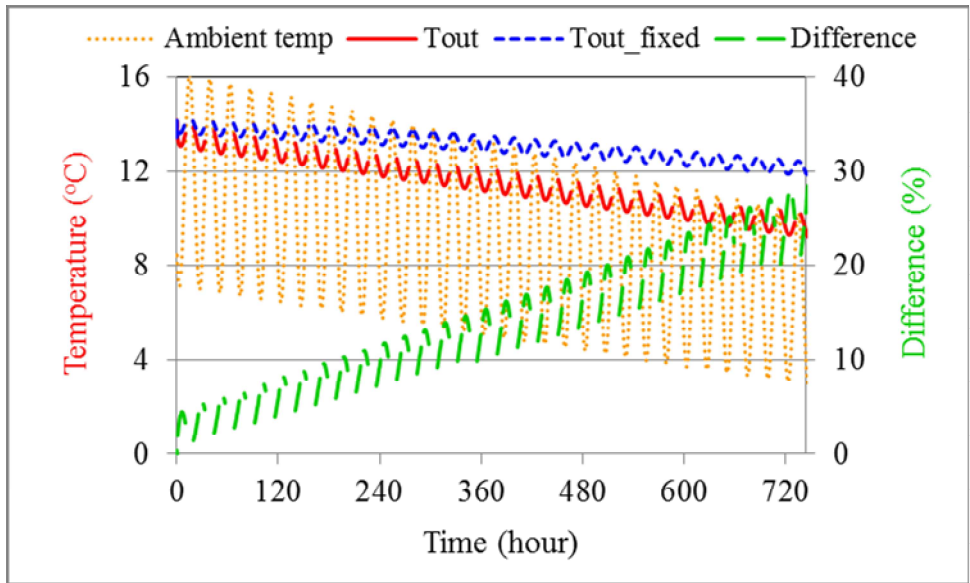


(b) Without interactions

Fig. 14 Predicted outlet air temperature for different heat exchanger lengths

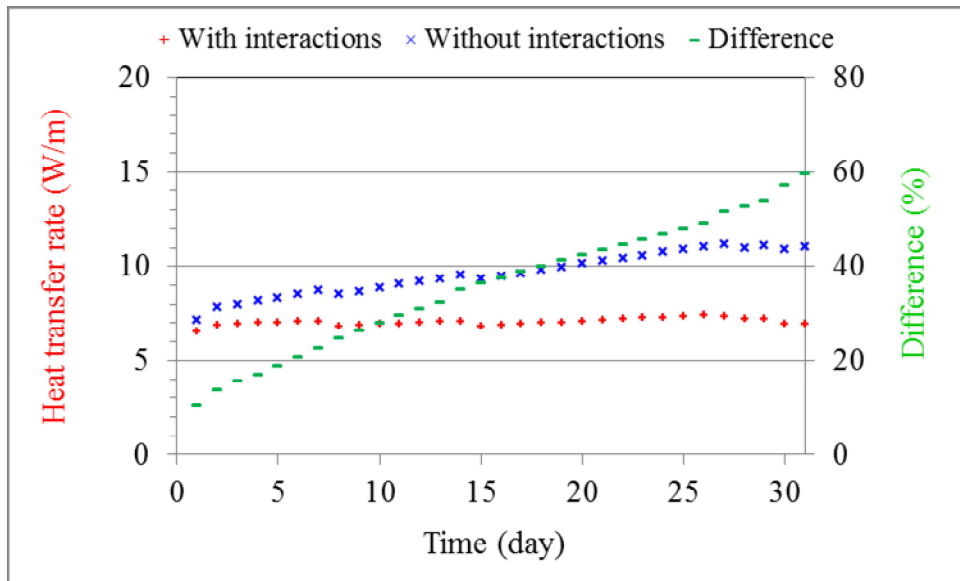


(a) Pipe temperature (Tpipe with interactions, Tpipe\_fixed without interactions)

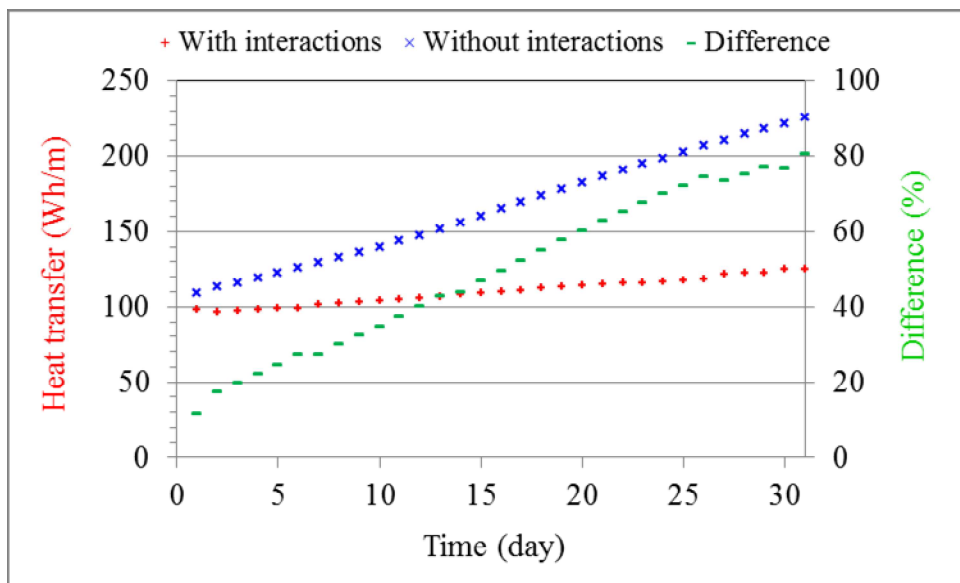


(b) Outlet air temperature, (Tout with interactions, Tout\_fixed without interactions)

Fig. 15 Predicted variations with time of pipe and supply air temperatures for a 40 m long heat exchanger



(a) Daily mean heat transfer rate



(b) Daily heat transfer

Fig. 16 Predicted heat transfer for a 40 m long heat exchanger